REVIEW
Lattice dynamics of iron chalcogenides: Raman scattering study

MARKO R. OPAČIĆ[1,2]* and NENAD Ž. LAZAREVIĆ[2]

[1]Faculty of Electrical Engineering, Bulevar Kralja Aleksandra 73, University of Belgrade, Belgrade, Serbia and [2]Center for Solid State Physics and New Materials, Institute of Physics, Pregrevica 118, University of Belgrade, Belgrade, Serbia

Abstract: The discovery of superconductivity in FeSe led to a new subclass of high-temperature superconductors – iron chalcogenides. Materials from this group exhibit variety of specific features, from superconductivity with relatively high critical temperatures to low-dimensional magnetic properties. This review presents the most important results regarding the iron chalcogenides, with special emphasis on their vibrational properties investigated by means of Raman spectroscopy. Temperature- and/or doping-dependent Raman scattering spectra of iron chalcogenides provide a valuable insight into the complex relationships between the vibrational, electronic and magnetic properties of these materials. The results presented in this review demonstrated that Raman spectroscopy provides new insights which may significantly improve our understanding of the fundamental properties of iron chalcogenides.

Keywords: superconductors; phonons; energy; linewidth.

CONTENTS

957

1. INTRODUCTION

Superconductivity (SC) is one of the greatest and the most striking phenomena discovered so far in the materials science. The history of SC began in 1911, when Kamerlingh-Onnes observed it in mercury below 4 K.[1] Since then, researchers made a great effort in searching for materials with as high as possible superconducting critical temperature T_c.

The breakthrough in the development of SC materials happened with the discovery of SC in oxide compounds. In 1975, $Ba(Pb,Bi)O_3$ was reported with $T_c \approx 13$ K,[2] which motivated further intensive studies. These investigations resulted in the discovery of SC in $La_{2-x}Ba_xCuO_2$ system ($T_c = 35$ K) – the first high-temperature superconductor,[3] as well as in $YBa_2Cu_3O_{7-x}$ compound ($T_c = 92$ K).[4] Numerous SC materials from this class were found in quick succession, from which $HgBa_2Ca_2Cu_3O_8$ ($T_c = 134$ K) should be mentioned.[5] All cuprate superconductors have distorted, oxygen-deficient, multi-layered perovskite structure. The most important property is an alternating multi-layer of CuO_2 planes, with intercalated layers containing Y, Ba, La, Sr,..., which act to stabilize the structure and to dope the carriers onto the CuO_2.[6–8] This structure causes a large anisotropy in normal conducting and superconducting properties.[6,8] Parent (undoped) compounds are Mott insulators, with long range antiferromagnetic (AFM) order at low temperatures.[7,8] Similarities between the AFM state of the undoped materials and doping-induced SC state indicate that the electron–electron interaction is more significant than electron-phonon interaction, making the SC unconventional.[9,10] It was argued that cuprates have d-wave pairing symmetry and one Fermi surface sheet.[11]

The first iron-based superconductor was discovered in 2006 (LaFePO, $T_c = 5$ K).[12] However, until 2008, when Kamihara et $al.$[13] found SC in $LaFeAsO_{1-x}F_x$ with $T_c = 26$ K (43 K under high pressure), it was widely believed that only cuprates belong to the class of unconventional high-T_c superconductors. This discovery led to a new class of the so-called iron pnictide SC which includes several types of materials, denoted according to their crystal structure: 1111-compounds (LaFePO, LaFeAsO, $SmFeAsO_{1-x}$ with $T_c = 56$ K[14]), 122-family ($Ba_{0.6}K_{0.4}Fe_2As_2$ with $T_c = 38$ K[15]), 111-compounds (MFeAs, $T_c = 18$ K[16]), etc. Crystal structure of these superconductors is given in Fig. 1. All these materials crystallize into the [FeAs]-layered structure, with spacer or charge reservoir blocks between the FeAs-layers.[17,18] The parent compounds are poor metals and it is widely believed that proximity to the magnetically ordered states induces SC, making them unconventional, like in the cuprates.[17,18] However, in iron pnictides SC and AFM order can coexist, contrary to the cuprates, where SC state emerges only after the AFM order is destroyed by doping.[18,19] Symmetry of the pairing wave function can be of the $s^{\pm}$-type,[20,21] although this is still under intensive debate.
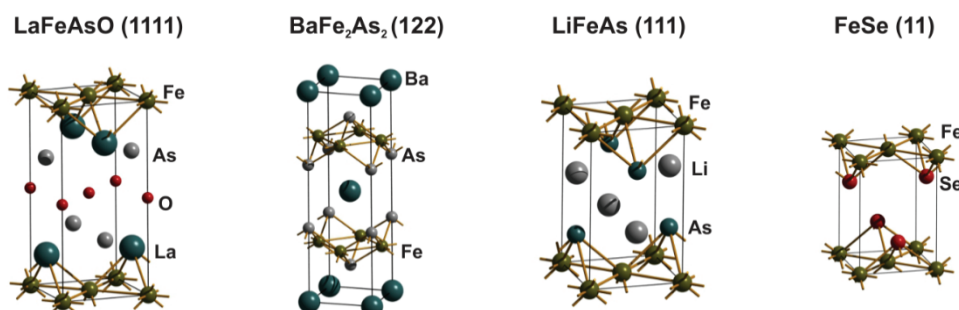
Fig. 1. Crystal structure of the representative iron-based superconductors.

FeSe is the first discovered material from one of the newest subclasses of iron-based superconductors – iron chalcogenides.[22] Its physical properties are extremely sensitive to doping on the chalcogen site, as well as to the Fe concentration, and T_c can be enhanced by applying pressure.[23,24] Intercalation of alkali metal between the FeSe layers led to the formation of $A_xFe_{2-y}Se_2$ (A = alkali metal) crystals with the defect 122* structure.[25] These materials exhibit very interesting properties, including the presence of AFM phase with ordered vacancies and vacancy-free SC/semiconducting phase, unconventional superconductivity with $T_c > 30$ K and large iron magnetic moments.[25–28] Absence of hole pockets at the Fermi surface suggests that the pairing mechanism may differ from the one in the pnictides. By cutting the layers of $FeSe_4$ tetrahedra, *e.g.*, removing every third Fe atom from these layers, one obtains a basic building block of the so-called spin-ladder compounds $BaFe_2Se_3$ ($BaFe_2S_3$).[29] These compounds have low-dimensional magnetic properties, which opened a new field in searching for new iron-based materials.[30–33]

In this article an overview of iron-chalcogenides is presented, but instead of a comprehensive review of their features, we focus our attention on the vibrational properties studied by Raman spectroscopy, as a suitable technique for investigating lattice and magnetic excitations of crystalline solids. It can also provide valuable information about coupling of phonons with electrons and charge-density waves and might even serve as a useful tool for probing the crystal symmetry.[34–36]

2. 11-TYPE MATERIALS

2.1. Crystal structure

Materials with the general formula FeCh (Ch = Se or Te), belonging to this group, have the simplest structure among all iron chalcogenides. They are built of edge-sharing $FeCh_4$ tetrahedra stacked along the crystallographic *c*-axis, see Fig. 1. At room temperature, they adopt the tetragonal crystal structure of the PbO type, space group *P4/nmm*.[22,37,38]

The crystal structure of FeSe at low temperatures is orthorombic, space group *Cmma*,[24,37,39] although it was initially proposed that $FeSe_{0.88}$ below $T_s \approx$ ≈ 100 K changes symmetry into triclinic, space group $P\text{-}\bar{1}$.[22] Structural transition temperature T_s for FeSe differs between various papers, depending strongly on the strain and sample stoichiometry.[37,40,41] Based on the temperature evolution of synchrotron X-ray diffraction profiles of $FeSe_{0.92}$,[37] it is concluded that T_s is about 70 K, whereas elsewhere[40] is showed that the phase transition in SC $Fe_{1.01}Se$ occurs at 90 K.

With Te-doping of FeSe crystals, the tetragonal-to-orthorombic structural transition moves toward lower temperatures and finally disappears for $FeTe_{0.507}Se_{0.493}$.[42] For low Te-content a miscible region with the local phase separation between two phases emerges.[23,43] These two phases have the same space group (*P4/nmm*) but different lattice parameters. With further increasing Te-concentration, the monoclinic structure appears at low temperatures (space group $P2_1/m$), instead of orthorombic.[38] Martinelli e*t al.*[38] reported tetragonal-to-monoclinic phase transition in $Fe_{1+y}Te_{1-x}Se_x$ crystals for $x \leq 0.1$, with increasing T_s as x decreases. For the end member $Fe_{1+y}Te$, the structural transition occurs around 70 K.

2.2. Physical properties

FeSe exhibits metallic behavior of electrical resistivity (ρ) from room temperature down to $T_c \approx 8$ K, where a sharp drop to zero resistance occurs.[22,23,43] Some authors[22] noticed a weak anomaly at about 100 K, which coincide with the anomaly in magnetic susceptibility $\chi(T)$, and attributed them to the structural transition. They observed almost temperature independent magnetic susceptibility for $T > T_c$, which led them to conclude that FeSe does not order magnetically.[22] However, recent inelastic neutron scattering experiments revealed stripe and Neel spin fluctuations over a wide energy range.[44] Susceptibility measurements also showed SC transition at about 8 K.[22,43] Temperature dependence of resistivity under various pressures is analyzed,[24] and the SC transition was noticed below 13.4 K for low pressures. With the increasing pressure, T_c rapidly increases and reaches maximal value of 37 K at about 6.6 GPa. With further pressurization, T_c decreases and at 13.9 GPa $T_c \approx 6$ K.[24] It was recently shown that an electronic nematic state develops below T_s,[45,46] suggesting that structural transition in FeSe may be driven by the orbital, magnetic and/or charge instability.

FeTe does not exhibit the SC transition.[38,43] Its resistivity weakly increases with decreasing temperature and exhibits an upturn at about 77 K, with rapid drop. Below the structural phase transition temperature $T_s = 70$ K FeTe has metallic behaviour.[38,43] Structural transition is followed by the AFM spin ordering, with $T_N \approx T_s$.[42] For $FeTe_{0.82}$ single crystals, magnetic susceptibility curve $\chi(T)$ exhibits two anomalies, at 65 and 125 K. Anomalous peak in $\rho(T)$ also appears at 65 K.[23] It was later shown that this behaviour is connected with the structural and

AFM phase transition.[47] Hall constant, R_H, is negative in the temperature range 10 K $\leq T \leq$ 160 K, indicating that charge carriers are dominantly electrons.[23]

Comprehensive study of physical properties of Fe(Se$_{1-x}$Te$_x$)$_{0.82}$, $0 \leq x \leq 1$, alloys is performed.[23] Maximal T_c of about 14 K is achieved for the sample with $x = 0.6$, and SC disappears in the end member ($x = 1$). Anomaly in the susceptibility at 125 K, similar to that in FeTe$_{0.82}$, persists for all samples with $x > 0.4$. It was shown that,[47] for the (FeSe$_{0.4}$Te$_{0.6}$)$_{0.82}$ sample, short range magnetic correlations appear below 75 K and rapidly enhance below 40 K, which coincide with anomalous temperature dependence of R_H in this temperature range, indicating the strong interplay between spin and charge degrees of freedom.[23] Samples with $0 \leq x \leq 0.15$ have metallic resistivity from room temperature down to T_c, whereas samples with $0.3 \leq x \leq 1$ have a weak upturn before approaching the SC transition temperature.[23] This is consistent with the results for FeTe$_{1-x}$Se$_x$, $0 < x \leq 0.2$, alloys,[38] where all samples show an upturn in $\rho(T)$ below 100 K, which weakens and shifts to lower temperature as x increases, and metallic behavior at lower temperatures. For $x \geq 0.05$, material become SC, and T_c increases with increasing Se content.[38] Similar resistivity curves were also obtained for FeSe$_{1-x}$Te$_x$ samples with low Se content, where it was found that T_c increases with x for $x \leq 0.75$, and $T_{c,max}$ = 15.3 K for $x = 0.25$.[43]

2.3. Raman scattering studies

According to the factor group analysis (FGA) for the *P4/nmm* space group, four Raman active modes (A$_{1g}$+B$_{1g}$+2E$_g$) could be observed in the room-temperature Raman spectra of FeCh (Ch = Se or Te) materials. A$_{1g}$ mode represents vibrations of the Ch-ions, whereas B$_{1g}$ one represents Fe-ion vibrations along the *z*-axis. Twofold degenerate E$_g$ modes originate from Fe- and Ch-ion vibrations within the *ab*-plane.[39,48]

Vibrational properties of 11-iron chalcogenides were extensively studied by means of Raman spectroscopy.[48–52] Almost all authors observed and assigned, at room temperature, two Raman active modes, of A$_{1g}$ and B$_{1g}$ symmetry, allowed by the selection rules when measuring from the (001)-plane of the sample. The A$_{1g}$ mode was not observed in Fe$_{1.03}$Se$_{0.3}$Te$_{0.7}$ sample,[49] although in FeTe$_{0.92}$ sample it is present; it was suggested that it may be due to the vacancies introduced into the system with Se doping, or slightly different excess of Fe-ions. Energies of the A$_{1g}$ and B$_{1g}$ modes for different samples are compared in Table I. As can be seen, they are rather close. However, temperature dependence of Raman mode energy, $\omega(T)$, and linewidth, $\Gamma(T)$, differs substantially between various papers. The spectrum of FeSe single crystal,[39] is shown in Fig. 2.

Magnetic transition that exists in FeTe leaves a clear fingerprint on the behavior of B$_{1g}$ mode energy and linewidth.[48,50,52] Namely, the B$_{1g}$ mode exhibits significant softening and narrowing below $T_N \approx 70$ K (where it changes the sym-

metry to A_g[52]) for all samples except $Fe_{1.09}Te$. Besides that, both the B_{1g} mode energy and linewidth decrease with decreasing temperature[48,50,52] (Fig. 3) and it was shown[52] that they scales well with the normalized magnetic susceptibility, confirming that spin-phonon coupling substantially influence the behaviour of the $B_{1g}(Fe)$ mode.

TABLE I. Experimentally obtained energies of the A_{1g} and B_{1g} Raman modes at room temperature (except for FeSe,[51] for which data are shown at $T = 5$ K) for some FeCh single crystals

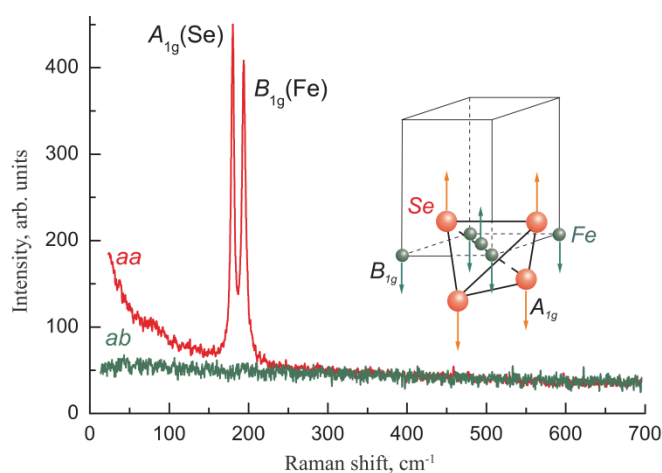| Wave number	$Fe_{1.05}Te$[48]	$Fe_{1.07}Te$[52]	$FeTe_{0.92}$[49]	$FeTe_{0.6}Se_{0.4}$[51]	FeSe[39]
$\bar{v}$ (A_{1g}) / cm^{-1}	155.2	156	159.1	161	179.8
$\bar{v}$ (B_{1g}) / cm^{-1}	201.4	198	196.3	202	193.9

Fig. 2. Polarized Raman scattering spectra of FeSe, room temperature. The inset shows the displacement patterns of the observed modes.[39] (Reprinted with permission from Ref. 39, copyright (2013) by the American Physical Society).

Absence of the B_{1g} phonon softening below T_N for $Fe_{1.09}Te$ single crystal[50] was ascribed to the significant Fe excess, which contributes to the filling up the gap in the spin-wave excitation spectrum with the low-energy spin fluctuations. Unlike the B_{1g} one, behaviour of the A_{1g} symmetry mode differs substantially. The only common feature is the large intrinsic linewidth, which is attributed[48] to the spin-orbital frustration, whereas elsewhere[52] is suggested that electron–phonon interaction may also play an important role.

The A_{1g} mode for $Fe_{1.051}Te$[48] hardens and broadens with decreasing temperature, showing a weak anomaly in $\omega(T)$ at T_s, followed by more rapid increase of $\Gamma(T)$ below T_s. Authors believe that the A_{1g} mode energy renormalization is caused by the phonon modulation of the magnetic interactions and by the anti-phase motion of Te-ions surrounding Fe-ions, which modulates exchange interaction. Rapid increase of the A_{1g} mode linewidth is attributed to the spin-orbital

frustration. Energy and linewidth of the A_{1g} mode for $Fe_{1.02}Te$ and $Fe_{1.09}Te$[50] remains almost constant at the temperatures up to 300 K. The A_{1g} mode energy and linewidth were analyzed[52] using phonon anharmonicity model and good agreement is obtained between experimental data and calculated spectra, indicating that they follow anharmonic temperature dependence.
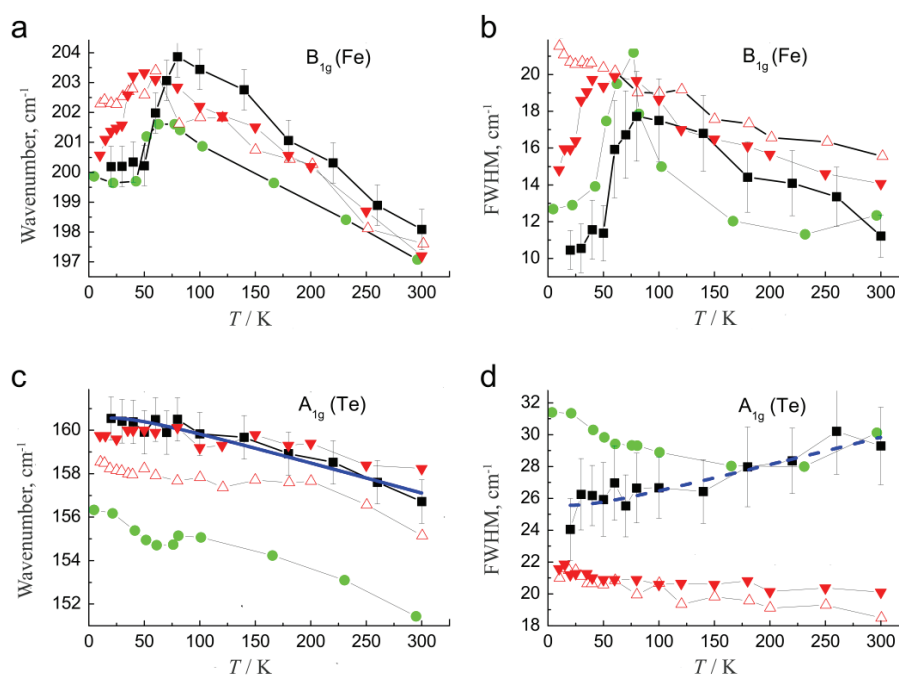

Fig. 3. Comparison of energy and linewidth temperature dependence for A_{1g} and B_{1g} Raman active modes of $Fe_{1+y}Te$ crystals. Filled circles represent data from Ref. 48, open triangles data from Ref. 50, $y = 0.09$, filled triangles data from Ref. 50, $y = 0.02$, and filled squares data from Ref. 52. Solid and dashed lines are calculated spectra using phonon anharmonicity model. (Reprinted from Ref. 52, copyright (2017) with permission from Elsevier).

Effect of Se doping on FeTe Raman spectra has also been investigated.[49,50,52] Um *et al.*[50] analyzed Raman spectra of Se-doped FeTe single crystals and showed that in the sample with the highest Se content ($Fe_{0.95}Te_{0.56}Se_{0.44}$) change of the A_{1g} and B_{1g} mode energy and linewidth with temperature is in agreement with the anharmonic picture: the phonon energy increases and the linewidth decreases with the decreasing temperature. By decreasing Se content, the energy and the linewidth of these modes gradually moves away from the conventional behaviour and for the $Fe_{1.00}Te_{0.78}Se_{0.22}$ crystal the B_{1g} phonon even broadens with decreasing temperature (Fig. 4). Absence of phonon renormalization at T_c for these SC samples is expected because their energies are much larger than the energy of the SC gap.[50]
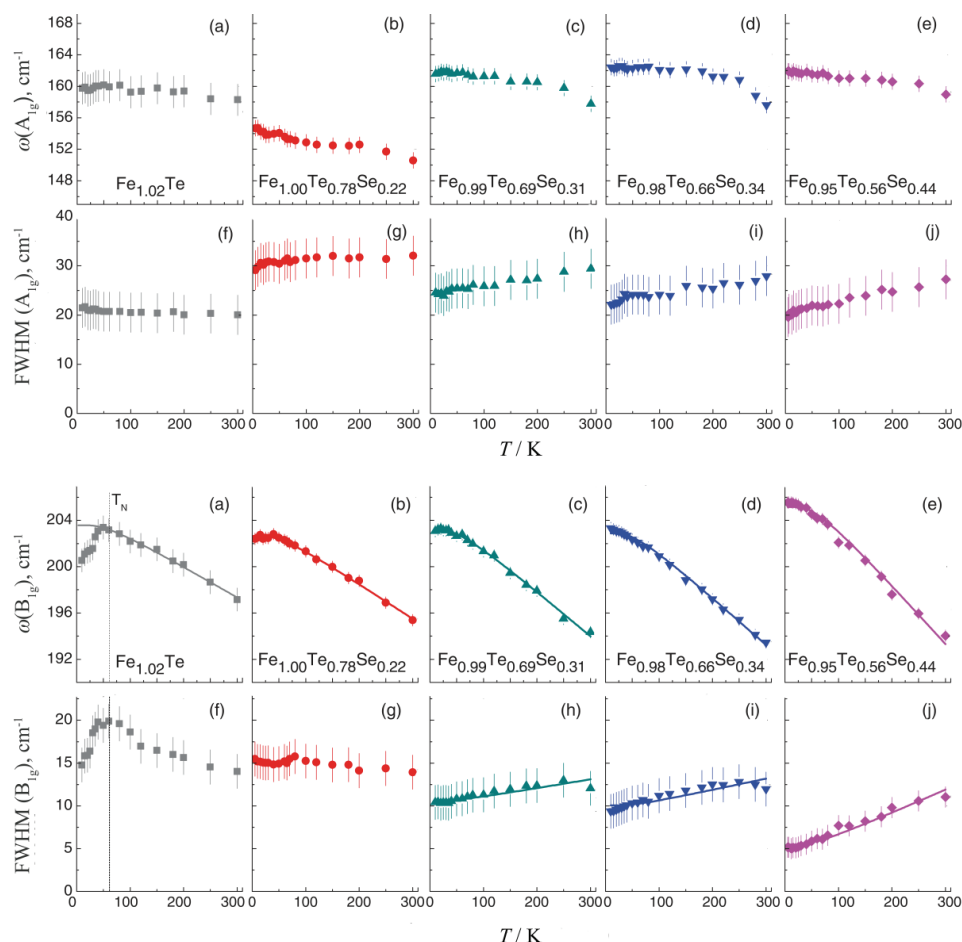
Fig. 4. Temperature dependence of the A_{1g} and B_{1g} mode frequency (ω) and f linewidth (FWHM) of the $Fe_{1.02}Te$, $Fe_{1.00}Te_{0.78}Se_{0.22}$, $Fe_{0.99}Te_{0.69}Se_{0.31}$, $Fe_{0.98}Te_{0.66}Se_{0.34}$ and $Fe_{0.95}Te_{0.56}Se_{0.44}$ samples.[50] (Reprinted with permission from Ref. 50, copyright (2012) by the American Physical Society).

More detailed analysis of the B_{1g} mode linewidth temperature dependence for Se-doped samples revealed that with decreasing Se content its intrinsic linewidth increases, which is attributed to the influence of the spin-phonon coupling, since lower Se (higher Te) content means stronger magnetic interactions. Raman spectra of Se-doped $Fe_{1+y}Te$ crystals were analyzed[52] with respect to the undoped case. It was observed that the A_{1g} and B_{1g} modes have opposite behaviour of energy and linewidth with Se doping: A_{1g} mode hardens and narrows whereas the B_{1g} one softens and broadens with increasing Se content. A_{1g} mode hardening is explained by the mass effect, whereas decreased linewidth is attributed to the lower electron–phonon interaction and/or to the excess Fe-ions. On the other

hand, B_{1g} mode broadening in $Fe_{1.02}Te_{0.6}Se_{0.4}$ compared with $Fe_{1.07}Te$ authors ascribed to the induced structural disorder, whereas phonon softening could be explained with the change in excess iron in these two single crystals. Qualitatively similar behaviour is presented[50] for the A_{1g} mode, whereas for the B_{1g} one the situation is almost opposite.

Temperature-dependent phonon Raman spectra of FeSe were analyzed in detail.[39] Room-temperature spectra consist of A_{1g} and B_{1g} modes, as expected from the selection rules. Due to the structural transition into the ortorhombic phase (*e.g.*, lowering of the rotational symmetry from C4 to C2), A_{1g} mode changes symmetry becoming A_g one, but without energy change, and three new modes appearing at higher energies can be of B_{2g}/B_{3g} symmetry, according to the *Cmma* space group. They emerge due to the splitting of E_g mode from the tetragonal phase. Both A_{1g} and B_{1g} mode energies vary smoothly with temperature, and large B_{1g} mode hardening with decreasing temperature is argued to be a consequence of the dynamical crossover from Fe spin state $S = 2$ to $S = 0$ with the lowering of temperature.[39] They suggested that smooth temperature dependence of the phonon linewidth at T_s indicates that orbital fluctuations do not have significant impact on the behavior of Raman modes. Highly polarized quasi-elastic response emerging in Raman spectra of the tetragonal phase, with maximal intensity at T_s, is considered as a fingerprint of electronic nematic fluctuations.[39,53] E_g mode splitting to $B_{2g}+B_{3g}$ phonons in FeSe, as a consequence of C4-symmetry breaking, is found to be only about 2.6 cm^{-1}, which is small in comparison to $Ba(Fe_{1-x}Co_x)_2As_2$, probably due to the lack of the magnetic order (Fig. 5).[54] This
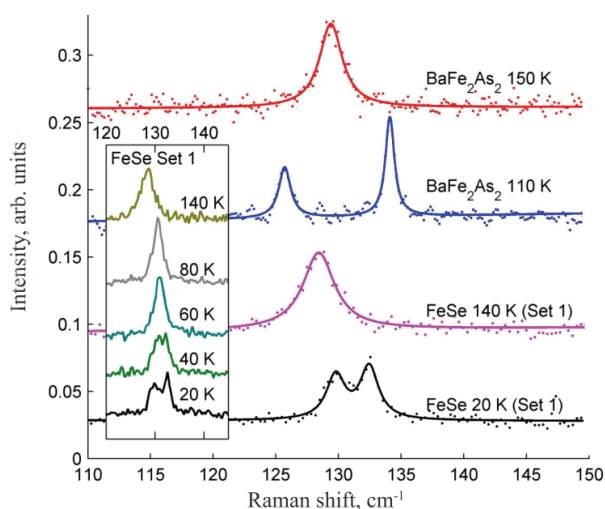

Fig. 5. Raman spectra of $BaFe_2As_2$ and FeSe single crystals. The inset shows temperature dependence of the FeSe Raman spectrum near 130 cm^{-1}, vertically offset for clarity.[54] (Reprinted with permission from Ref. 54, copyright (2016) by the American Physical Society).

splitting sets in below 65 K, where the spin-lattice relaxation rate is found to increase, which led to the conclusion that spin correlations have stronger influence to the lattice than the orbital interactions.[46]

3. 122*-TYPE MATERIALS

3.1. Crystal structure

The SC in this class was firstly discovered in a sample with the nominal composition $K_{0.8}Fe_2Se_2$, with the proposed tetragonal crystal structure of the $ThCr_2Si_2$-type, space group *I4/mmm*.[25] It consists of FeSe layers and K atoms stacked alternatively along the *z*-axis (Fig. 6a). Intercalation of the K atoms between the FeSe slabs significantly increases the lattice parameter *c* (decreasing
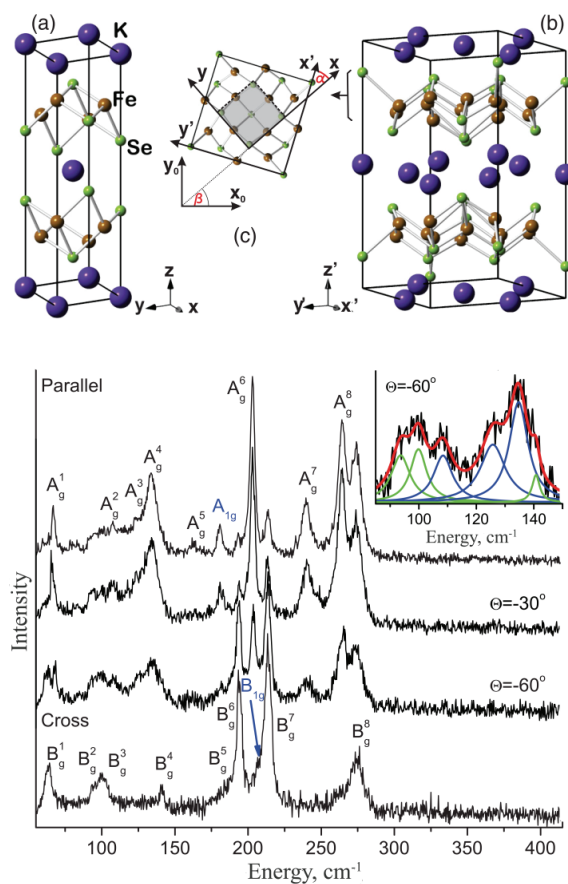

Fig. 6. Crystal structure of $K_xFe_{2-y}Se_2$ within: a) *I4/mmm* and b) *I4/m* unit cells; c) FeSe layer in the (001)-plane of the sample. The solid line represents *I4/m*, whereas shaded square illustrates *I4/mmm* unit cell. Angle between principal axes of the two phases is around 26.6°. Parallel: Raman spectra of $K_xFe_{2-y}Se_2$ measured at 85 K in various polarization configuration ($\Theta = \sphericalangle(\mathbf{e_i},\mathbf{e_s})$).[28]

dimensionality of the system), as well as the interlayer Fe–Fe spacing. $(Fe_2Se_2)^{\delta-}$ layers serve as conducting layers, whereas K^+ are charge carriers. Fe–Se–Fe bond angle is very close to the angle of the ideal tetrahedra (109.47°).[25]

However, the appearance of additional peaks in the neutron powder diffraction (NPD) spectra indicated that symmetry lowering to *I4/m* phase occurs, due to the Fe vacancies ordered into the √5×√5 superlattice in the FeSe plane (Fig. 6b).[26] Zavalij *et al.*[55] and Wang *et al.*[56] also suggested √5×√5 order of the iron vacancies. Fe vacancy order disappears at very high temperature (500 K $\leq T_s \leq$ $\leq$ 578 K), depending on the sample composition,[26,57] and *I4/mmm* symmetry is achieved.

The application of the transmission electron microscopy, Chen *et al.*[58] showed that $K_xFe_{2-y}Se_2$ single crystals exhibit a mesoscopic phase separation between an insulating phase with √5×√5 vacancy order and SC/semiconducting phase free of vacancies (*i.e.*, with composition KFe_2Se_2, space group *I4/mmm*). This is also seen by Li e*t al.*[27] on $K_xFe_{2-y}Se_2$ thin films. PXRD measurements confirmed[28] the phase separation: experimental data were well described with the mixture of *I4/m* and *I4/mmm* space groups. Presence of both phases was also confirmed by Raman scattering measurements.[28,59–61] On the other hand, Bao *et al.*[62] reported phase separation between three phases (*I4/m*, *I4/mmm* and *Pmna*) in $K_xFe_{2-y}Se_2$ samples for $1.4 \leq 2–y \leq 1.6$ and $x > 0.85$ (the samples have general formula $K_2Fe_3Se_4$) between T_s and $T^* \approx 350$ K, whereas below T^* only *I4/m* phase with ordered Fe vacancies persists. For Fe content $1.6 \leq 2–y \leq 1.7$ the sample composition is described with $K_2Fe_4Se_5$ and below T_s their space group is *I4/m*.[62]

Doping of $K_xFe_{2-y}Se_2$ crystals on either chalcogen or transition metal site significantly affects their properties. It was recently shown[60] that the phase separation persists in Co-doped $K_xFe_{2-y}Se_2$ single crystals. However, when Co content is significant ($z \geq 0.92$ in $K_xFe_{2-y-z}Co_zSe_2$), vacancy order was not observed and these samples belong to the *I4/mmm* space group.[60,63,64] Doping of $K_xFe_{2-y}Se_2$ with small Ni content also preserves the phase separation.[59] Similarly to the Co--doped case, in $K_xFe_{2-y-z}Ni_zSe_2$ samples with $z \geq 0.73$ low symmetry *I4/m* phase disappears.[59] Pure $K_xNi_{2-y}Se_2$ crystallizes in the tetragonal crystal structure with *I4/mmm* space group, without any indications of vacancy ordering,[65–67] as well as his Co-counterpart. $K_xFe_{2-y}Se_2$ samples doped with S on chalcogen site exhibit iron vacancy order for all doping levels.[68,69]

3.2. Physical properties

Detailed investigations revealed that the physical properties of $K_xFe_{2-y}Se_2$ strongly depend on the sample composition, *i.e.*, K- and Fe-stoichiometry. Bao *et al.*[62] systematically studied few samples having general formula $K_xFe_{2-y}Se_2$ and obtained different properties for various sample compositions. Two samples with higher Fe and lower K content exhibit SC with $T_c \approx 30$ K and large resistivity just

above T_c. These samples show poor diamagnetic response below T_c. With the gradually increasing K content, a bump in $\rho(T)$ appears, which is attributed to the metal–insulator crossover, similarly to the results presented elsewhere:[25] above the peak, samples show semiconducting behaviour, whereas below the bump down to T_c, $\rho(T)$ has typical metallic character. Peak position is strongly dependent on the sample composition.[25,62] With the further increasing of K and the decreasing of Fe content, the gradual opening of transport activation gap was observed in the resistivity.[62]

Early studies of the magnetic properties of alkali metal iron selenides revealed that AFM order appears at $T_N \approx 560$ K, slightly below the Fe vacancy ordering temperature T_s.[26,62] The four magnetic moments from the nearest neighbouring Fe atoms order ferromagnetically (FM), whereas these FM blocks form the block-checkerboard AFM order, with very high magnetic moment (3.31 μ_B/Fe at 11 K).[26] SC transition strongly affects the magnetic order parameter, suggesting significant interaction between SC and AFM order.[26]

Recent studies indicated that SC in $K_xFe_{2-y}Se_2$ was highly influenced by the connectivity between SC phases and the proximity effects.[70,71] Three $K_xFe_{2-y}Se_2$ samples with different microstructure exhibited different T_c,[71] although they all have approximately the same fractional ratio of the SC area and similar resistive and magnetic properties. Huang *et al.*[71] showed that proximity effects, that is, the interlayer hopping and interlayer spin coupling, reduce T_c from the theoretically predicted 65 K to the experimentally observed 32 K. On the other hand, large AFM order results in a large SC order, thus explaining relatively high T_c.[71]

The chemical doping is an appropriate way to tune and control physical properties of materials, since it introduces changes in the structure and carrier density. Doping on the Fe site with other transition metals is detrimental for SC.[72] Namely, Cr-, Co- and Zn-doping rapidly suppresses SC in the $K_{0.8}Fe_{2-y}Se_2$, by inducing a large effective magnetic moment, thus destroying SC *via* a magnetic pair-breaking effect.[72] Recently reported study of Ni-doped $K_xFe_{2-y}Se_2$ single crystals[59] shows that small Ni content destroys SC, leading to the insulating behaviour, whereas with further Ni-doping metallic character of crystals gradually increases. It was also shown that these materials exhibit spin glass behaviour below critical temperature T_f of 10–50 K, depending on the Ni concentration.[59] $K_xNi_{2-y}Se_2$ have a local charge-density-wave state persisting up to 300 K.[65] Some authors[66] reported the metallic resistivity of $K_xNi_{2-y}Se_2$ single crystal up to the room temperature, without SC transition or bump in the $\rho(T)$, unlike the $K_xFe_{2-y}Se_2$. SC is suppressed probably due to the K and Ni deficiency, indicating the strong sensitivity to the sample composition. Magnetic measurements revealed that this material is Pauli paramagnet, with local magnetic moments much lower than in $K_xFe_{2-y}Se_2$.[66] Co-doped $K_xFe_{2-y}Se_2$ single crystals behave similarly to its Ni-counterparts.[60] Preliminary analysis of $K_xCo_{2-y}Se_2$ single crystals indi-

cate the FM phase transition at 74 K and absence of SC.[73] When S completely replaces Se in $K_xFe_{2-y}Se_2$, single crystal becomes a small-gap semiconductor, which is ascribed to the random scattering potential introduced by the Fe deficiency, and exhibits a spin glass behaviour below 32 K.[68,69]

3.3. Raman scattering studies

FGA for the *I4/m* space group predicts $9A_g$, $9B_g$ and $9E_g$ modes to be observed in the Raman scattering experiments,[28,61] whereas for the *I4/mmm* space group only four phonon modes ($A_{1g}+B_{1g}+2E_g$) are expected to be observed.[28,61,64,67] In most of the Raman scattering studies of $K_xFe_{2-y}Se_2$ single crystals, the phonon spectra with large number of modes are obtained, confirming the fact that Fe vacancy order reduces locally the symmetry to *I4/m*.[28,61,74–76] These spectra are very similar to each other; characteristic $K_xFe_{2-y}Se_2$ Raman spectrum is shown in Fig. 6. However, the symmetry analysis of the phonon spectra was performed assuming the different space groups in various papers. Temperature analysis of Raman spectra, as well as the line shape of some modes, also differs, as will be discussed.

First Raman study of $K_xFe_{2-y}Se_2$ was done by Zhang *et al.*[74] They assumed the *I4/m* space group for the single phase and thus assigned phonons which appeared in the parallel polarization configuration only as A_g symmetry modes, whereas those modes appearing in both polarization configurations were assigned as B_g ones. In that way 6 A_g and 5 B_g modes were assigned, with energies coinciding well with the lattice dynamics calculations. The most intriguing fact is a frequency jump at T_c for the Raman mode appearing at about 180 cm^{-1} in parallel polarization configuration, of unknown origin, since its energy did not match with any of the calculated A_g mode energies. Authors interpreted this behaviour as an evidence of specific connection between phonons and SC. This hardening was also observed,[75] where Raman spectra of three SC ($K_{0.8}Fe_{1.6}Se_2$, $Tl_{0.5}K_{0.3}Fe_{1.6}Se_2$ and $Tl_{0.5}Rb_{0.3}Fe_{1.6}Se_2$) and one non-SC sample ($KFe_{1.5}Se_2$) were analyzed in terms of *I4/m* space group (Fig. 7). It is suggested that this mode is local, originating from the nanoscopic region of filled Fe vacancies. By comparing the Raman spectra of $K_{0.8}Fe_{1.6}Se_2$ and $KFe_{1.5}Se_2$ single crystals, frequency shift of the Raman modes originating from Fe- and Se-ion vibrations was observed, due to the differences in the FeSe plane induced by the change of Fe content. Doping on the K site did not influence phonon spectra above 60 cm^{-1}, but induces additional modes in the low energy range, attributed to the change of local symmetry in the K layer.[75] *I4/m* space group is assumed also for $K_xFe_{2-y}Se_2$.[76] 16 Raman modes at room temperature was observed, some of them with Fano line shape, attributed to the coupling of the vibrations with AFM spin fluctuations. Authors agreed that three new phonon modes appear below 250 K, due to the structural transition, *i.e.* symmetry lowering from the *I4/m* to the *I4* phase.[76]
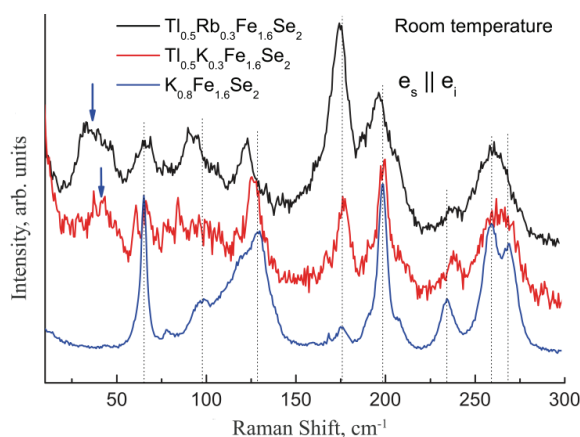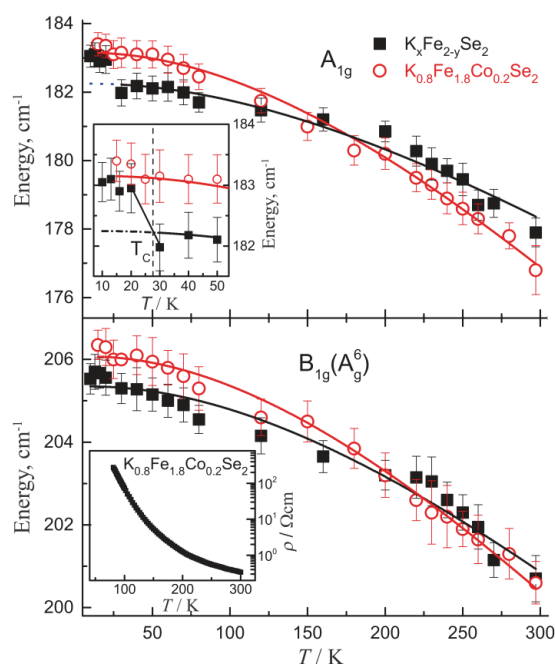
Fig. 7. Raman spectra of the three superconducting crystals measured at room temperature. Additional modes, appearing below 60 cm^{-1} in the Tl- and Rb-substituted samples, are denoted by blue arrows. Dotted lines are guides indicating the peak positions.[75] (Reprinted with permission from Ref. 75, copyright (2012) by the American Physical Society).

Unlike to the presentations by some authors,[74–76] Raman spectra of K$_x$Fe$_{2–y}$Se$_2$ were analyzed[28,61] in terms of both *I4/m* and *I4/mmm* space groups. Raman modes from the *I4/mmm* space group were assigned.[28] It was determined that the A$_{1g}$ mode appears at about 180 cm^{-1}, whereas energy of the B$_{1g}$ mode is 207 cm^{-1}. It is interesting to note that this A$_{1g}$ phonon is probably the same Raman mode as that of the unknown origin,[74,75] with frequency jump at T_c. Large number of modes from the low symmetry *I4/m* phase were assigned[28] by means of detailed symmetry analysis and measurements in various polarization configurations. A$_g$ and B$_g$ mode energies coincide with other data,[74] which can be seen from Table II. Detailed temperature-dependent Raman scattering study of SC K$_x$Fe$_{2–y}$Se$_2$ and non-SC K$_x$Fe$_{1.8}$Co$_{0.2}$Se$_2$ is given.[61] Similar spectra of the two crystals indicate that phase separation is preserved with small amount of Co doped at the Fe-site. Analysis of the temperature-dependent Raman spectra revealed the phonon energies temperature dependence is dominantly driven by the lattice thermal expansion, whereas the impact of phonon anharmonicity is negligible. The renormalization of the A$_{1g}$ phonon energy below T_c was observed only for the SC sample (Fig. 8), which led to the conclusion that it is induced by the SC gap opening, in line with the theoretically expected behaviour.[77]

Room temperature Raman spectra of Ni- and Co-doped K$_x$Fe$_{2–y}$Se$_2$ crystals give valuable insight into the structural changes of K$_x$Fe$_{2–y}$Se$_2$ with doping. Recent Raman studies[59,60] revealed that increasing Co and Ni content have similar influence on phonon spectra of these materials. When Ni (Co) content is low, large number of modes are present in Raman spectra (Fig. 9), in accordance with the symmetry lowering due to the Fe-vacancy ordering, *i.e.*, presence of *I4/m* phase,

TABLE II. Comparison of experimentally observed wavenumbers (in cm^{-1}) at room temperature for the selected A_g and B_g symmetry modes of $K_xFe_{2-y}Se_2$ single crystals[28,74]

Ref.	A_g^4	A_g^6	A_g^8	B_g^7	B_g^8
28	134	203	264	214	274
74	134.6	202.9	264.6	214.3	274.9

Fig. 8. Temperature dependence of A_{1g} and B_{1g} mode energy in $K_xFe_{2-y}Se_2$ and $K_{0.8}Fe_{1.8}Co_{0.2}Se_2$ single crystals. Inset: An enlarged view of A_{1g} temperature dependence in a low temperature region near T_c.[61]

as in pure $K_xFe_{2-y}Se_2$.[28] Broad asymmetric structures, appearing in Raman spectra of both series of samples for the intermediate Ni (Co) concentrations, were attributed to the large structural disorder. At high Ni (Co) concentrations, as well as for pure $K_xNi_{2-y}Se_2$[67] and $K_xCo_{2-y}Se_2$,[64] only two modes can be observed in Raman spectra, confirming the lack of any vacancy order. Appearance of the A_{1g} mode in the whole series gives a clear evidence that *I4/mmm* phase persists for all Ni (Co) concentrations.[59,60] Detailed Raman scattering studies of $K_xNi_{2-y}Se_2$[67] and $K_xCo_{2-y}Se_2$ single crystals[64] support the findings given elsewhere.[59,60] As opposed to the A_{1g} phonon that appears at similar energies in these two compounds,[64,67] the B_{1g} phonon energy (representing vibrations of the transition metal ions) differs substantially (Table III). Besides that, by measuring from the (010)-plane of $K_xNi_{2-y}Se_2$, one E_g mode is clearly observed (Fig. 10) whereas the other, low intensity E_g mode, was confirmed by numerical calculations. Large intrinsic line-
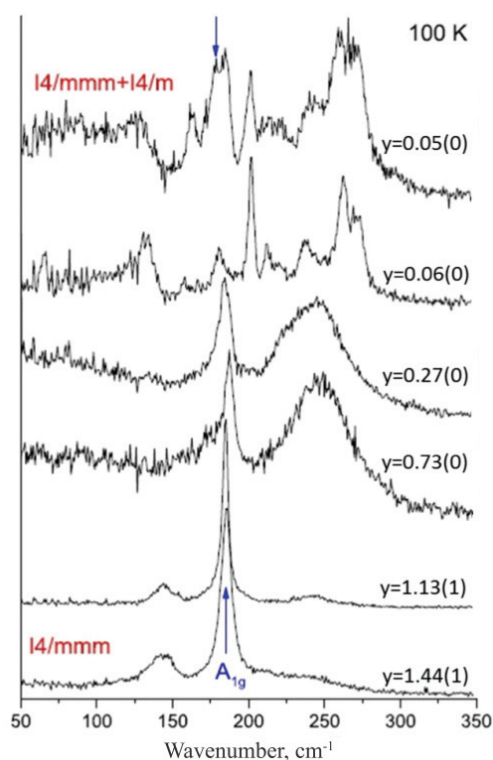
Fig. 9. Raman spectra of $K_xFe_{2-x-y}Ni_ySe_2$ single crystal series measured from the (001)-plane at 100 K.[59]

width of the B_{1g} phonon, together with the mode asymmetry, is believed to originate from the structural disorder, although the impact of the electron–phonon interaction cannot be excluded.[67] Similar features of the B_{1g} phonon are also observed in $K_xCo_{2-y}Se_2$, where it was argued that they are mainly caused by the spin fluctuations coupled to the electronic structure *via* lattice vibrations.[64] Temperature dependence of A_{1g} and B_{1g} mode energy in $K_xCo_{2-y}Se_2$ in the paramagnetic phase is governed by the lattice thermal expansion and phonon anharmonicity, whose relative importance is not yet firmly established. Change of phonon linewidths is well described with the lattice anharmonicity model. Both phonon modes have energy jump below the FM transition temperature T_c, but the A_{1g} mode exhibits sharpening with further cooling, whereas the B_{1g} mode broadens (Fig. 11). Sudden frequency change of the observed Raman mode energies as the sample gets magnetized can occur due to the magnetostriction effects, spin-phonon coupling and/or changes in the electron–phonon interaction caused by the spin polarization and changes in the electronic spectrum.[64]

As opposed to $K_x(Co, Ni)_{2-y}Se_2$, phonon spectra of $K_{0.88}Fe_{1.63}S_2$ consists of large number of modes, originating from the *I4/m* phase. This confirms symmetry lowering due to the Fe-vacancy order, but without phase separation, unlike the

$K_xFe_{2-y}Se_2$.[78] 6 A_g and 8 B_g modes were assigned by measuring the spectra from the (001)-plane of the sample.

TABLE III. Experimentally obtained energies of the A_{1g} and B_{1g} Raman modes (in cm^{-1}) at room temperature for $K_xM_{2-y}Se_2$ single crystals (M = Fe, Co or Ni)

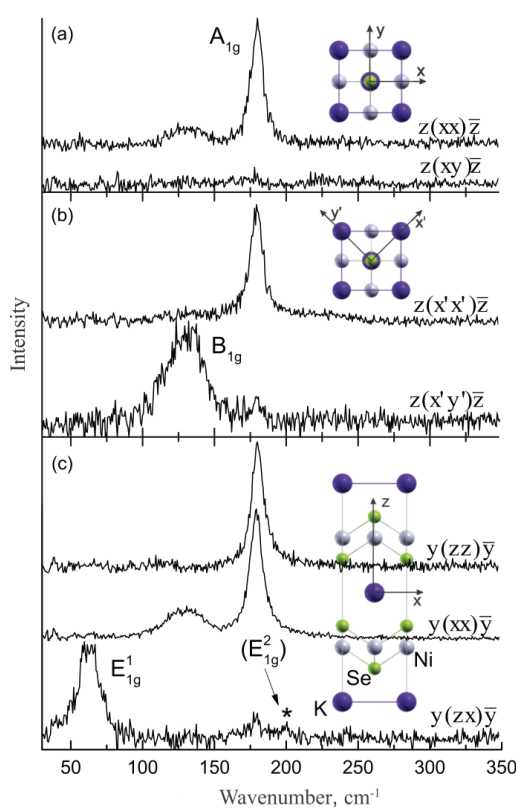| Wave number	$K_xFe_{2-y}Se_2$[28]	$K_xCo_{2-y}Se_2$[64]	$K_xNi_{2-y}Se_2$[67]
$\omega(A_{1g})$	180	197	178
$\omega(B_{1g})$	207	187	134

Fig. 10. Room temperature Raman spectra of $K_{0.95}Ni_{1.86}Se_2$ single crystals measured in various scattering configurations ($\mathbf{x}$ = [100], $\mathbf{y}$ = [010], $\mathbf{x'}$ = $= 1/\sqrt{2}$ [110], $\mathbf{y'}$ = $1\sqrt{2}$ /[1 1 0], $\mathbf{z}$ = $= b[001]$).[67]

4. IRON-BASED SPIN-LADDER MATERIALS

4.1. Crystal structure

The most studied materials among the iron-containing spin-ladder compounds with the general formula AFe_2X_3 (A = K, Rb, Cs, Ba and X = Ch) are barium–iron-chalcogenides, $BaFe_2(S,Se)_3$. The ladder structure of these compounds can be considered as obtained by cutting the layers of edge-sharing $FeSe_4$ tetrahedra of the two-dimensional 11-iron chalcogenides, *i.e.*, removing every third Fe atom from the FeSe layers. $BaFe_2(S,Se)_3$ crystals consists of one-dimensional
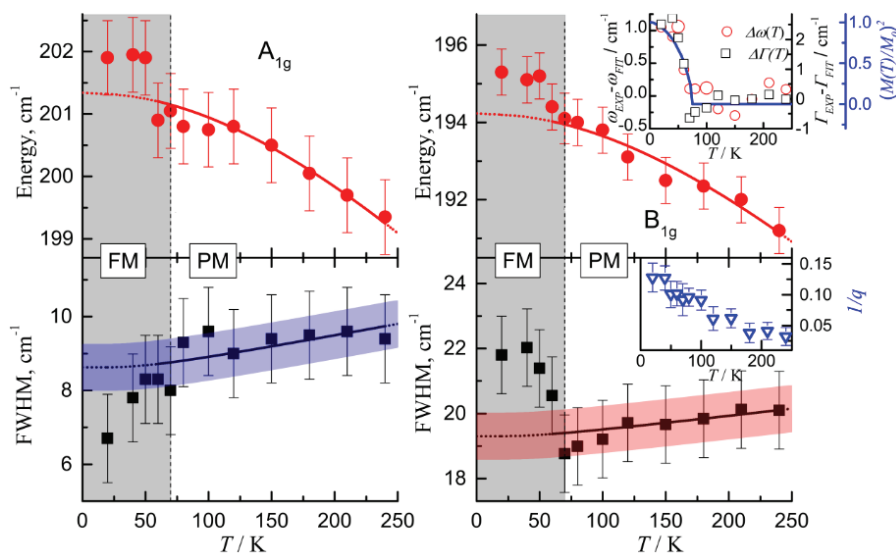
Fig. 11. Temperature dependence of the energy and linewidth (FWHM) for the A_{1g} and B_{1g} Raman modes of $K_xCo_{2-y}Se_2$ single crystal. Solid lines are the theoretical fits which take into account lattice thermal expansion and phonon–phonon scattering for energy and linewidth temperature dependence, respectively. The dotted lines are the extrapolation to 0 K. Shaded area denotes temperature range of the ferromagnetic phase. Inset of B_{1g} energy: temperature dependence of the B_{1g} mode frequency, compared with $(M(T)/M(0))^2$ curve. Inset of B_{1g} FWHM: measure of the electron–phonon coupling ($1/q$) of the B_{1g} mode as a function of temperature.[64]

$[Fe_2(S,Se)_3]^{2-}$ double chains, propagating along the long ladder direction (,,lag'') and Ba^{2+} as separators (Fig. 12). In $BaFe_2S_3$ the double chains extend along the a-axis, whereas in $BaFe_2Se_3$ the ladder lag is along the b-axis.[33,79] There are two important structural differences between these two materials. Namely, two different Fe–Fe distances along the ladder lag exist in $BaFe_2Se_3$, whereas in $BaFe_2S_3$ all Fe–Fe distances are the same. Moreover, $[Fe_2Se_3]^{2-}$ double chains are tilted off the bc-plane, with opposite tilting directions of the two neighbouring layers, whereas in $BaFe_2S_3$ there is no tilting. Due to the slight structural differences, $BaFe_2Se_3$ and $BaFe_2S_3$ crystals, although both orthorhombic, are not isostructural. $BaFe_2S_3$ has *Cmcm* space group, whereas space group of $BaFe_2Se_3$ is *Pnma*, both with four formula units per unit cell.[79]

$BaFe_2Se_2O$ is the first layered iron-oxychalcogenide with alkali earth metal. It consists of Fe–Se(O) layers and Ba^{2+}, stacked alternatively along the c-axis, similar with $BaFe_2Se_3$ and $BaFe_2S_3$. Fe–Se(O) double chains are bridged by the oxygen atoms along the a-axis and propagate along the b-axis. However, the intralayer structure differs from those in previously described spin-ladder materials. Different Fe–Se and Fe–O distances cause Fe atoms to be located in highly dis-

torted (asymmetric) tetrahedra, whose angle significantly deviates from the ideal value. Crystal structure is orthorombic (*Pmmn* space group), with two formula units per unit cell.[80]
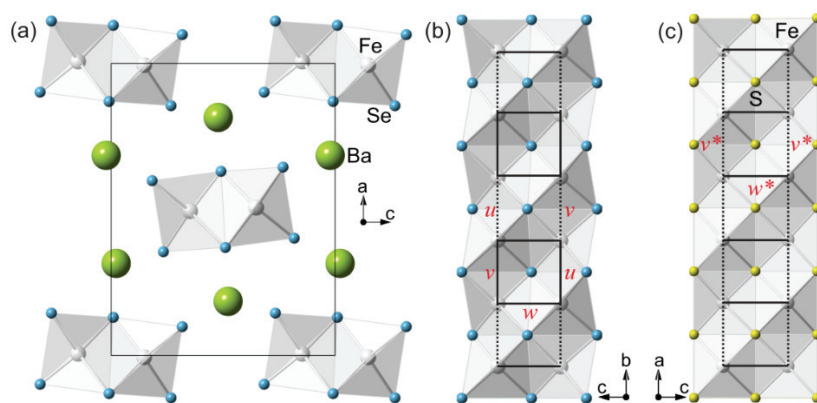

Fig. 12. Crystal structure of $BaFe_2Se_3$ and $BaFe_2S_3$. a) Projection of the $BaFe_2Se_3$ crystal in the (010)-plane; b) double chain of $[Fe_2Se_3]^{2-}$ tetrahedra propagating along the *b*-axis; c) $[Fe_2S_3]^{2-}$ double chain in the (010) plane. *w* and w^* denote Fe–Fe distances along short ladder directions ("rungs"), whereas *u*, *v* and v^* represent Fe–Fe distances along the ladder legs.[81]

4.2. Physical properties

$BaFe_2S_3$ has semiconducting $\rho(T)$, with very low resistivity.[82,83] The change of slope in resistivity occurs at about 275 K,[82] where inverse molar magnetic susceptibility has a broad hump.[83] This material also exhibits negative magneto-resistive effect of about 10 % at low temperatures. The divergence between ZFC (zero field-cooled) and and FC (field-cooled) magnetic susceptibility below 25 K points out to the spin-glass behaviour, which is confirmed by other measurements.[83] Strong intrachain AFM coupling of the ions, together with the additional crystal field splitting due to the neighbouring Fe atoms and direct Fe–Fe interactions cause ground state with $S = 0$.[83] Takahashi *et al.*[30] recently measured the resistivity of $BaFe_2S_3$ single crystals under various pressures and found the gradual suppression of insulating behaviour with increasing pressure, with metal––insulator transition at about 11 GPa. With further increasing pressure, this material exhibits SC below $T_c = 14$ K. The increased metallicity of the sample at higher pressures is caused by the anisotropic compression of the crystal.[30] NPD measurements indicate the stripe-type magnetic order, with magnetic moment 1.2 μ_B (at 4 K) per Fe site. These moments form FM units along the rung direction, whereas these units order antiferromagnetically along the lag direction.[30]

$BaFe_2Se_3$ single crystal also has semiconducting $\rho(T)$ properties, similar to $BaFe_2S_3$, but without magnetoresistive effect.[33] Large diversity of susceptibilities for different field directions indicatesmagnetic anisotropy.[29,33] The transition in

magnetic susceptibility at 255 K for all field directions is attributed to the cross-over from short-range to long-range AFM order.[33] This transition was not observed,[29] since a divergence of ZFC and FC magnetic susceptibilities is attributed to the spin-glass behavior with $T_f \approx 50$ K.

Resistivity measurements on $BaFe_2Se_2O$ single crystals revealed the insulating behaviour. At $T_a = 240$ K, there is anomaly in resistivity, allowing their fitting below T_a with the relation $\rho = \rho_0 \exp\{(E_a/k_BT)^\alpha\}$, $\alpha < 1$, which means that thermal activation is less effective at low temperatures and the other mechanism is responsible for electron trapping.[80] Authors proposed the existence of long range AFM order below 240 K, which is confirmed by the strong peak in differential magnetic susceptibility $\partial\chi/\partial T$ at T_a. Anisotropy in the magnetic susceptibility indicates that the easy axis of magnetization is in the ab-plane. Besides that, a sudden decrease of susceptibility below 115 K, with much less anisotropy, was attributed to the spin-singlet dimers, believed to be formed at low temperatures.[80] All iron ions in $BaFe_2Se_2O$ are in Fe^{2+} state and high spin state, and this compound can be considered as $S = 2$ spin-ladder system, with the dominant AFM superexchange interaction along the ladder rungs.[32]

4.3. Raman scattering studies

Raman spectra of $BaFe_2Se_2O$ were analysed.[31] In the optical part of the spectra 6 (of 6) A_g modes and 2 out of 2 B_{1g} modes were observed and assigned (Fig. 13) whereas the remaining modes (of B_{2g} and B_{3g} symmetry) could not be observed by measuring from the (001)-plane of the sample. Three new modes appearing below $T_N = 240$ K are attributed to the crystal structure and/or crystal symmetry change. Analysis of the Raman mode energy and linewidth depend-
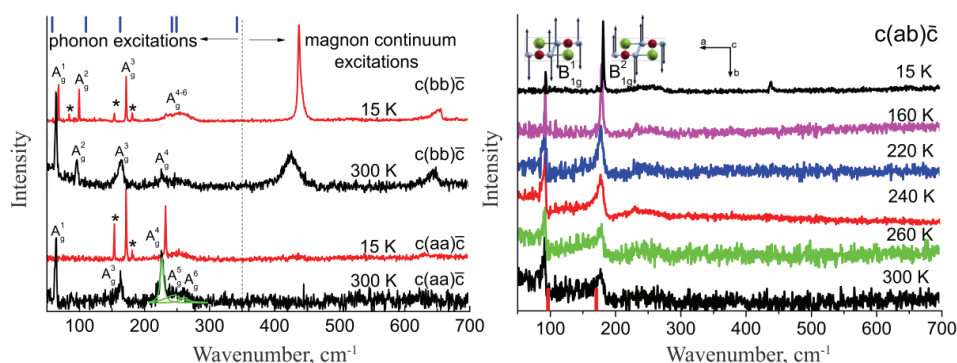

Fig. 13. Left: the (aa) and (bb) polarized Raman spectra of $BaFe_2Se_2O$ single crystals measured at room temperature and at 15 K. Vertical bars denote calculated values of the A_g Raman active modes. New modes appearing below 240 K are denoted by asterisks. Right: the (ab) polarized Raman spectra of $BaFe_2Se_2O$ single crystals measured at various temperatures. Vertical bars denote calculated values of the B_{1g} symmetry modes. Insets show normal modes of the two B_{1g} symmetry vibrations.[31]

ence on temperature showed significant hardening and narrowing of A_g modes below T_N. B_{1g} modes asymmetry above T_N (persisting in the region of short-range magnetic order) is believed to originate from the spin fluctuations.[31]

Besides the optical phonon modes, two broad and asymmetric structures appear in the Raman spectra of $BaFe_2Se_2O$ single crystals at higher energies, in $c(bb)\bar{c}$ polarization only (which coincides with the spin orientations). Therefore, they are assigned as two-magnon continuum modes.[31] These structures are shown in Fig. 14. From the ratio $T_N/T_{max} = 0.53$ (where T_{max} denotes temperature where magnetic susceptibility has a maximum), it was concluded that $BaFe_2Se_2O$ is a quasi-2D magnetic system. From the onset of the magnetic continuum, which should correspond to $2\Delta_S$ (where Δ_S is a spin gap energy), it was estimated $\Delta_S \approx$ ≈ 27 meV. Magnon modes disappear above 623 K, $e.g.$, 2.6 T_N[31] in agreement with the other results indicating that the short-range magnetic order in oxychalcogenides persists at least up to 2 T_N.[84]
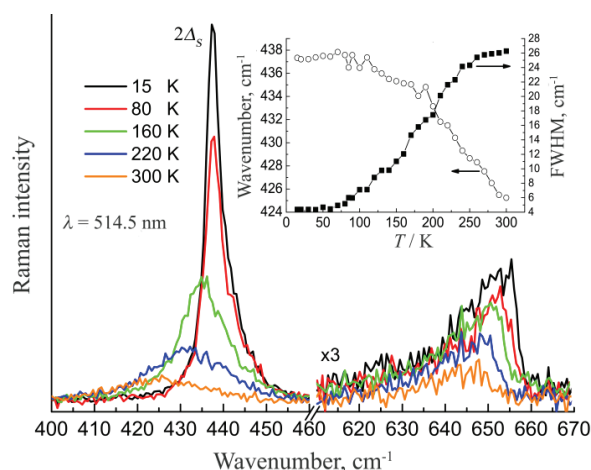

Fig. 14. Raman scattering spectra of $BaFe_2Se_2O$ single crystals measured at various temperatures between 15 and 300 K in $c(bb)\bar{c}$ polarization configuration. Only 400–670 cm^{-1} spectral range is shown. Inset: energy (circles) and linewidth (squares) of the $2\Delta_S$ (spin gap) mode as a function of temperature.[31]

Phonon properties of $BaFe_2S_3$ and $BaFe_2Se_3$ were analysed.[81] By measuring from the (110)-plane of the $BaFe_2S_3$ sample, in parallel polarization configurations 5 (of 5) A_g symmetry modes and 5 out of 6 B_{1g}, the symmetry modes were clearly observed. In crossed polarization configuration B_{2g} and B_{3g} modes could appear in the Raman spectra; therefore, the assignation was done with the help of lattice dynamics calculations. Three such modes were observed in phonon spectra.

On the other hand, lower symmetry of $BaFe_2Se_3$ single crystals compared to $BaFe_2S_3$, caused more Raman active modes to be observed in the phonon spectra. Indeed, by measuring from the (100)-plane of the sample, 9 (of 11) A_g symmetry

modes were observed in parallel polarization configuration, whereas in the crossed one three additional modes were assigned as of B_{3g} symmetry.[81]

The temperature analysis of phonon energy and linewidth was performed in terms of lattice thermal expansion and phonon anharmonicity for both $BaFe_2S_3$ and $BaFe_2Se_3$ single crystals. It turned out that the contribution of the phonon––phonon scattering to the Raman mode energy temperature dependence is negligible. The sudden change of slope of energy and linewidth temperature dependence of the A_g^4 mode at about 275 K (where the hump in inverse molar magnetic susceptibility and change of slope in resistivity also occur) in $BaFe_2S_3$ is attributed to the AFM spin ordering within the ladder lag from the short-range to the long-range state, without spin ordering of the whole crystal, followed by the change in the electronic structure. The energies of the all analyzed modes in $BaFe_2Se_3$ sharply increase below T_N, which was ascribed to the spin–phonon coupling. This mechanism is also responsible for the deviation from the usual anharmonic behaviour of the phonon linewidth.[81]

5. SUMMARY AND CONCLUSIONS

The results discussed in this review clearly demonstrate that Raman spectroscopy is a very powerful technique for investigating the vibrational properties of iron chalcogenides. Moreover, almost all structural and magnetic transitions leave a clear fingerprint on the vibrational spectra of 11, $122^{\divideontimes}$ and spin-ladder iron-based superconductors, reviewed in this article, through the appearance of new phonon modes or a sudden change in the phonon energy and/or linewidth.

Raman spectra of Fe(Te, Se) single crystals measured from the *ab*-plane consist of two modes, assigned as A_{1g} and B_{1g} ones. Magnetic transition in FeTe causes softening and narrowing of the B_{1g} (Fe) mode. With Se doping of FeTe crystals the A_{1g} mode hardens and narrows, whereas the B_{1g} ones softens and broadens, compared to the pure FeTe. Large B_{1g} mode hardening observed for FeSe is explained as a consequence of the dynamical crossover between different Fe spin states. Electronic nematic fluctuations leave a fingerprint through highly polarized quasielastic response in the Raman spectra of FeSe in the tetragonal phase.

Vibrational spectra of $K_xFe_{2-y}Se_2$ single crystals have large number of phonon peaks. Some authors assigned them according only to the *I4/m* space group, whereas the others assume the existence of *I4/mmm* and *I4/m* phases, which is confirmed by the other techniques. Renormalization of the A_{1g} mode energy at T_c in SC $K_xFe_{2-y}Se_2$ and the absence of renormalization in non-SC isostructural $K_xFe_{1.8}Co_{0.2}Se_2$ indicates that it is induced by the opening of SC gap, confirming that this mode indeed represents the *I4/mmm* phase vibration. Raman studies also revealed that doping of $K_xFe_{2-y}Se_2$ single crystals with different amount of Co and Ni significantly affects their crystal structure. When Ni (Co) content is low, large number of modes points out to the presence of both *I4/mmm* and *I4/m*

phases. At high dopant concentrations, as well as for pure $K_x(Co, Ni)_{2-y}Se_2$, only two modes, of A_{1g} and B_{1g} symmetry, appear in phonon spectra, confirming the lack of ordered vacancies. Spin-dependent electron-phonon coupling and magnetostriction effects leave a clear fingerprint on the vibrational spectra of $K_xCo_{2-y}Se_2$, through a strong deviations of the phonon energy and the linewidth temperature dependence from the anharmonic behaviour.

The magnetic ordering manifests itself through the impact on energy, linewidth and lineshape of the observed phonon modes of spin-ladder iron-based systems $BaFe_2S_3$, $BaFe_2Se_3$ and $BaFe_2Se_2O$. Besides that, the analysis of the two-magnon continuum modes of $BaFe_2Se_2O$ allows the estimation of the spin gap energy and classification of this material as a quasi-2D magnetic system.

Future work could be concentrated on the high pressure Raman scattering studies, as well as on the investigations of possible new materials from this class that will be produced by the doping of the existing ones. The results presented in this paper show that Raman spectroscopy is an invaluable tool which can expand our knowledge of the fundamental properties of iron chalcogenides.

И З В О Д

ДИНАМИКА РЕШЕТКЕ ГВОЖЂЕ-ХАЛКОГЕНИДА – ИСПИТИВАЊА МЕТОДОМ РАМАНОВЕ СПЕКТРОСКОПИЈЕ

МАРКО Р. ОПАЧИЋ[1,2] и НЕНАД Ж. ЛАЗАРЕВИЋ[2]

[1]Елекȓроȓехнички факулȳеȓ Универзиȳеȓа у Беоȋраду, Булевар краља Александра 73, Беоȋрад и[2]Ценȓар за физику чврсȓоȋ сȓања и нове маȓеријале, Инсȓиȳуȓ за физику, Преȋревица 118, Беоȋрад

Откриће суперпроводног кристала FeSe значило је појаву нове подкласе високотемпературских суперпроводника – гвожђе-халкогенида. Материјали из ове групе имају разна специфична својства, од суперпроводљивости са релативно високим критичним температурама до нискодимензионалних магнетних особина. Овај прегледни рад приказује најважније резултате везане за гвожђе-халкогениде, са посебним нагласком на њихове вибрационе особине, испитиване методом Раманове спектроскопије. Раманови спектри гвожђе-халкогенида у зависности од температуре и допирања пружају значајан увид у комплексне везе између вибрационих, електронских и магнетних особина ових материјала. Резултати приказани у овом прегледном раду показују да Раманова спектроскопија пружа нове информације које могу значајно побољшати разумевање фундаменталних својстава гвожђе-халкогенида.

(Примљено 21. марта, ревидирано 2.јуна, прихваћено 5. јуна 2017)

REFERENCES

1. H. Kamerlingh Onnes, *Commun. Phys. Lab. Univ. Leiden* **120b** (April 1911), reprinted in *Proc. K. Ned. Akad. Wet.***13** (1911) 1274
2. A. W. Sleight, J. L. Gillson, P. E. Bierstedt, *Solid State Commun.* **17** (1975) 27
3. J. G. Bednorz, K. A. Müller, *Z. Angew. Phys., B* **64** (1986) 189

4. C. W. Chu, P. H. Hor, R. L. Meng, L. Gao, Z. J. Huang, Y. Q. Wang, *Phys. Rev. Lett.* **58** (1987) 908
5. C. W. Chu, P. H. Hor, R. L. Meng, L. Gao, Z. J. Huang, *Science* **235** (1987) 567
6. M. A. Kastner, R. J. Birgeneau, G. Shirane, Y. Endoh, *Rev. Mod. Phys.* **70** (1998) 897
7. P. A. Lee, N. Nagaosa, X.-G. Wen, *Rev. Mod. Phys.* **78** (2006) 17
8. E. Dagotto, *Rev. Mod. Phys.* **66** (1994) 763
9. P. Monthoux, A. V. Balatsky, D. Pines, *Phys. Rev. Lett.* **67** (1991) 3448
10. D. J. Scalapino, *Phys. Rep.* **250** (1995) 329
11. C. C. Tsuei, J. R. Kirtley, C. C. Chi, Lock-See Yu-Jahnes, A. Gupta, T. Shaw, J. Z. Sun, M. B. Ketchen, *Phys. Rev. Lett.* **73** (1994) 593
12. Y. Kamihara, H. Hiramatsu, M. Hirano, R. Kawamura, H. Yanagi, T. Kamiya, H. Hosono, *J. Am. Chem. Soc.* **128** (2006) 10012
13. Y. Kamihara, T. Watanabe, M. Hirano, H. Hosono, *J. Am. Chem. Soc.* **130** (2008) 3296
14. Z.-A. Ren, G.-C. Che, X.-L. Dong, J. Yang, W. Lu, W. Yi, X.-L. Shen, Z.-C. Li, L.-L. Sun, F. Zhou, *Europhys. Lett.* **83** (2008) 17002
15. M. Rotter, M. Tegel, D. Johrendt, *Phys. Rev. Lett.* **101** (2008) 107006
16. X. C. Wang, Q. Q. Liu, Y. X. Lv, W. B. Gao, L. X. Yang, R. C. Yu, F. Y. Li, C. Q. Jin, *Solid State Commun.* **148** (2008) 538
17. M. D. Lumsden, A. D. Christianson, *J. Phys.: Condens. Matter* **22** (2010) 203203
18. D. C. Johnston, *Adv. Phys.* **59** (2010) 803
19. H. Chen, Y. Ren, Y. Qiu, Wei Bao, R. H. Liu, G. Wu, T. Wu, Y. L. Xie, X. F. Wang, Q. Huang, X. H. Chen, *Europhys. Lett.* **85** (2009) 17006.
20. I. I. Mazin, D. J. Singh, M. D. Johannes, M. H. Du, *Phys. Rev. Lett.* **101** (2008) 057003
21. A. D. Christianson, E. A. Goremychkin, R. Osborn, S. Rosenkranz, M. D. Lumsden, C. D. Malliakas, I. S. Todorov, H. Claus, D. Y. Chung, M. G. Kanatzidis, R. I. Bewley, T. Guidi, *Nature* **456** (2008) 930
22. F.-C. Hsu, J.-Y. Luo, K.-W. Yeh, T.-K. Chen, T.-W. Huang, P.-M. Wu, Y.-C. Lee, Y.-L. Huang, Y.-Y.Chu, D.-C. Yan, M.-K. Wu, *Proc. Natl. Acad. Sci. U.S.A.* **105** (2008) 14262
23. M. H. Fang, H. M. Pham, B. Qian, T. J. Liu, E. K. Vehstedt, Y. Liu, L. Spinu, Z. Q. Mao, *Phys. Rev., B* **78** (2008) 224503
24. S. Margadonna, Y. Takabayashi, Y. Ohishi, Y. Mizuguchi, Y. Takano, T. Kagayama, T. Nikagawa, M. Takata, K. Prassides, *Phys. Rev., B* **80** (2009) 064506
25. J. Guo, S. Jin, G. Wang, S. Wang, K. Zhu, T. Zhou, M. He, X. Chen, *Phys. Rev., B* **82**(2010) 180520
26. W. Bao, Q. Huang, G. F. Chen, M. A. Green, D. M. Wang, J. B. He, X. Q. Wang, Y. Qiu, *Chin. Phys. Lett.* **28** (2011) 086104
27. W. Li, H. Ding, P. Deng, K. Chang, C. Song, K. He, L. Wang, X. Ma, J.-P. Hu, X. Chen, Q.-K. Xue, *Nat. Phys.* **8** (2012) 126
28. N. Lazarević, M. Abeykoon, P. W. Stephens, H. Lei, E. S. Bozin, C. Petrovic, Z. V. Popović, *Phys. Rev., B* **86** (2012) 054503
29. B. Saparov, S. Calder, B. Sipos, H. Cao, S. Chi, D. J. Singh, A. D. Christianson, M. D. Lumsden, A. S. Sefat, *Phys. Rev., B* **84** (2011) 180409
30. H. Takahashi, A. Sugimoto, Y. Nambu, T. Yamauchi, Y. Hirata, T. Kawakami, M. Avdeev, K. Matsubayashi, F. Du, C. Kawashima, H. Soeda, S. Nakano, Y. Uwatoko, Y. Ueda, T. J. Sato, K. Ohgushi, *Nat. Mater.* **14** (2015) 1008
31. Z. V. Popović, M. Šćepanović, N. Lazarević, M. M. Radonjić, D. Tanasković, H. Lei, C. Petrovic, *Phys. Rev., B* **89** (2014) 014301

32. H. Kabbour, E. Janod, B. Corraze, M. Danot, C. Lee, M. H. Whangbo, L. Cario, *J. Am. Chem. Soc.* **130** (2008) 8261

33. H. Lei, H. Ryu, A. I. Frenkel, C. Petrovic, *Phys. Rev., B* **84** (2011) 214511

34. N. Lazarević, E. S. Bozin, M. Šćepanović, M. Opačić, H. Lei, C. Petrovic, Z. V. Popović, *Phys. Rev., B* **89** (2015) 224301

35. N. Lazarević, Z. V. Popović, R. Hu, C. Petrovic, *Phys. Rev., B* **83** (2011) 024302

36. N. Lazarević, Z. V. Popović, R. Hu, C. Petrovic, *Phys. Rev., B* **81** (2010) 144302

37. S. Margadonna, Y. Takabayashi, M. T. McDonald, K. Kasperkiewicz, Y. Mizuguchi, Y. Takano, A. N. Fitch, E. Suarde, K. Prassides, *Chem. Commun.* (2008) 5607

38. A. Martinelli, A. Palenzona, M. Tropeano, C. Ferdeghini, M. Putti, M. R. Cimberle, T. D. Nguyen, M. Affronte, C. Ritter, *Phys. Rev., B* **81** (2010) 094115

39. V. Gnezdilov, Y. G. Pashkevich, P. Lemmens, D. Wulferding, T. Shevtsova, A. Gusev, D. Chareev, A. Vasiliev, *Phys. Rev., B* **87** (2013) 114305

40. T. M. McQueen, A. J. Williams, P. W. Stephens, J. Tao, Y. Zhu, V. Ksenofontov, F. Casper, C. Felser, R. J. Cava, *Phys. Rev. Lett.* **103** (2009) 057002

41. S.-H. Baek, D.V. Efremov, J. M. Ok, J. S. Kim, Jeroen van den Brink, B. Büchner, *Phys. Rev., B* **93** (2016) 180502(R)

42. S. Li, C. de la Cruz, Q. Huang, Y. Chen, J. W. Lynn, J. Hu, Y.-L. Huang, F.-C. Hsu, K.-W. Yeh, M.-K. Wu, P. Dai, *Phys. Rev., B* **79** (2009) 054503

43. Y.Mizuguchi, F.Tomioka, S.Tsuda, T.Yamaguchi, and Y.Takano, *J. Phys. Soc. Jpn.* **78** (2009) 074712

44. Qisi Wang, Yao Shen, Bingying Pan, Xiaowen Zhang, K. Ikeuchi, K. Iida, A. D. Christianson, H. C. Walker, D. T. Adroja, M. Abdel-Hafiez, Xiaojia Chen, D. A. Chareev, A. N. Vasiliev, Jun Zhao, *Nat. Commun.* **7** (2016) 12182

45. S-H. Baek, D. V. Efremov, J. M. Ok, J. S. Kim, Jeroen van den Brink, B. Büchner, *Nat. Mater.* **14** (2015) 210

46. M. D. Watson, T. K. Kim, A. A. Haghighirad, N. R. Davies, A. McCollam, A. Narayanan, S. F. Blake, Y. L. Chen, S. Ghannadzadeh, A. J. Schofield, M. Hoesch, C. Meingast, T. Wolf, A. I. Coldea, *Phys. Rev., B* **91** (2015) 155106

47. W. Bao, Y. Qiu, Q. Huang, M. A. Green, P. Zajdel, M. R. Fitzsimmons, M. Zhernenkov, S. Chang, M. H. Fang, B. Qian, E. K. Vehstedt, J. Yang, H. M. Pham, L. Spinu, Z. Q. Mao, *Phys. Rev. Lett.* **102** (2009) 247001

48. V. Gnezdilov, Y. Pashkevich, P. Lemmens, A. Gusev, K. Lamonova, T. Shevtsova, I. Vitebskiy, O. Afanasiev, S. Gnatchenko, V. Tsurkan, J. Deisenhofer, A. Loidl, *Phys. Rev., B* **83** (2011) 245127

49. T.-L. Xia, D. Hou, S. C. Zhao, A. M. Zhang, G. F. Chen, J. L. Luo, N. L. Wang, J. H. Wei, Z.-Y. Lu, Q. M. Zhang, *Phys. Rev., B* **79** (2009) 140510

50. Y. J. Um, A. Subedi, P. Toulemonde, A. Y. Ganin, L. Boeri, M. Rahlenbeck, Y. Liu, C. T. Lin, S. J. E. Carlsson, A. Sulpice, M. J. Rosseinsky, B. Keimer, M. Le Tacon, *Phys. Rev., B* **85**(2012) 064519

51. K. Okazaki, S. Sugai, S. Niitaka, H. Takagi, *Phys. Rev., B* **83** (2011) 035103

52. Z. V. Popović, N. Lazarević, S. Bogdanović, M. M. Radonjić, D. Tanasković, Rongwei Hu, Hechang Lei, C. Petrovic, *Solid State Commun.* **193** (2014) 51

53. P. Massat, D. Farina, I. Paul, S. Karlsson, P. Strobel, P. Toulemonde, M.-A. Measson, M. Cazayous, A. Sacuto, S. Kasahara, T. Shibauchi, Y. Matsuda, Y. Gallais, *Proc. Natl. Acad. Sci. U.S.A.* **113** (2016) 9177

54. Yuwen Hu, Xiao Ren, Rui Zhang, Huiqian Luo, Shigeru Kasahara, Tatsuya Watashige, Takasada Shibauchi, Pengcheng Dai, Yan Zhang, Yuji Matsuda, Yuan Li, *Phys. Rev., B* **93** (2016) 060504(R)
55. P. Zavalij, W. Bao, X. F. Wang, J. J. Ying, X. H. Chen, D. M. Wang, J. B. He, X. Q. Wang, G. F. Chen, P.-Y. Hsieh, Q. Huang, M. A. Green, *Phys. Rev., B* **83** (2011) 132509
56. Z. Wang, Y. J. Song, X. L. Shi, Z. W. Wang, Z. Chen, H. F. Tian, G. F. Chen, J. G. Guo, H. X. Yang, J. Q. Li, *Phys. Rev., B* **83** (2011) 140505(R)
57. F. Ye, S. Chi, W. Bao, X. F. Wang, J. J. Ying, X. H. Chen, H. D. Wang, C. H. Dong, M. H. Fang, *Phys. Rev. Lett.* **107** (2011) 137003
58. F. Chen, M. Xu, Q. Q. Ge, Y. Zhang, Z. R. Ye, L. X. Yang, Juan Jiang, B. P. Xie, R. C. Che, M. Zhang, A. F. Wang, X. H. Chen, D. W. Shen, J. P. Hu, D. L. Feng, *Phys. Rev. X* **1** (2011) 021020
59. Hyejin Ryu, Milinda Abeykoon, Kefeng Wang, Hechang Lei, N. Lazarević, J. B. Warren, E. S. Bozin, Z. V. Popović, C. Petrovic, *Phys. Rev., B* **91** (2015) 184503
60. Hyejin Ryu, Kefeng Wang, M. Opačić, N. Lazarević, J. B. Warren, Z. V. Popović, C. Petrovic, *Phys. Rev., B* **92** (2015) 174522
61. M. Opačić, N. Lazarević, M. Šćepanović, H. Ryu, H. Lei, C. Petrovic, Z. V. Popović, *J. Phys.: Cond. Matter* **27** (2015) 485701
62. W. Bao, G. N. Li, Q. Huang, G. F. Chen, J. B. He, M. A. Green, Y. Qiu, D. M. Wang, J. L. Luo, M. M. Wu, *Chin. Phys. Lett.* **30** (2013) 027402
63. G. Huan, M. Greenblatt, *J. Less-Common Met.* **156** (1989) 247
64. M. Opačić, N. Lazarević, M. M. Radonjić, M. Šćepanović, H. Ryu, A. Wang, D. Tanasković, C. Petrovic, Z. V. Popović, *J. Phys.: Cond. Matter* **28** (2016) 485401
65. J. R. Neilson, A. Llobet, A. V. Stier, L. Wu, J. Wen, J. Tao, Y. Zhu, Z. B. Tesanovic, N. P. Armitage, T. M. McQueen, *Phys. Rev., B* **86** (2012) 054512
66. H. Lei, M. Abeykoon, K. Wang, E. S. Bozin, H. Ryu, D. Graf, J. B. Warren, C. Petrovic, *J. Phys.: Cond. Matter* **26** (2014) 015701
67. N. Lazarević, M. Radonjić, M. Šćepanović, H. Lei, D. Tanasković, C. Petrovic, Z. V. Popović, *Phys. Rev., B* **87** (2013) 144305
68. H. Lei, M. Abeykoon, E. S. Bozin, K. Wang, J. B. Warren, C. Petrovic, *Phys. Rev. Lett.* **107** (2011) 137002
69. H. Lei, M. Abeykoon, E. S. Bozin, C. Petrovic, *Phys. Rev., B* **83** (2011) 180503(R)
70. X. Ding, D. Fang, Z. Wang, H. Yang, J. Liu, Q. Deng, G. Ma, C. Meng, Y. Hu, H.-H. Wen, *Nat. Commun.* **4** (2013) 1897
71. S.-M. Huang, C.-Y. Mou, T.-K. Lee, *Phys. Rev., B* **88** (2013) 174510
72. D. Tan, C. Zhang, C. Xi, L. Ling, L. Zhang, W. Ton, Y. Yu, G. Feng, H. Yu, L. Pi, Z. Yang, S. Tan, Y. Zhang, *Phys. Rev., B* **84** (2011) 014502
73. J. Yang, B. Chen, H. Wang, Q. Mao, M. Imai, K. Yoshimura, M. Fang, *Phys. Rev., B* **88** (2013) 064406
74. A. M. Zhang, K. Liu, J. H. Xiao, J. B. He, D. M. Wang, G. F. Chen, B. Normand, Q. M. Zhang, *Phys. Rev., B* **85** (2012) 024518
75. A. M. Zhang, K. Liu, J. B. He, D. M. Wang, G. F. Chen, B. Normand, Q. M. Zhang, *Phys. Rev., B* **86** (2012) 134502
76. A. Ignatov, A. Kumar, P. Lubik, R. H. Yuan, W. T. Guo, N. L. Wang, K. Rabe, G. Blumberg, *Phys. Rev., B* **86** (2012) 134107
77. M. Cardona, *NATO ASI Ser., B* **372** (2002) 257.
78. N. Lazarević, H. Lei, C. Petrovic, Z. V. Popović, *Phys. Rev., B* **84** (2011) 214305
79. H. Hong, H. Steinfink, *J. Solid State Chem.* **5** (1972) 93

80. H. Lei, H. Ryu, V. Ivanovski, J. B. Warren, A. I. Frenkel, B. Cekic, W.-G. Yin, C. Petrovic, *Phys. Rev., B* **86** (2012) 195133

81. Z. V. Popović, M. Šćepanović, N. Lazarević, M. Opačić, M. M. Radonjić, D. Tanasković, H. Lei, C. Petrovic, *Phys. Rev., B* **91** (2015) 064303

82. W. Reiff, I. Grey, A. Fan, Z. Eliezer, H. Steinfink, *J. Solid State Chem.* **13** (1975) 32

83. Z. S. Gönen, P. Fournier, V. Smolyaninova, R. Greene, F. M. Araujo-Moreira, B. Eichhorn, *Chem. Mater.* **12** (2000) 3331

84. J. B. He, D. M. Wang, H. L. Shi, H. X. Yang, J. Q. Li, G. F. Chen, *Phys. Rev., B* **84** (2011) 205212.